

GT2011-458- +

NOVEL CONCEPT FOR AN AIR-PRESSURE DRIVEN MICRO-TURBINE FOR POWER GENERATION

Michele Focchi

Istituto Italiano di Tecnologia
Genova, Italia
michele.focchi@iit.it

Emanuele Guglielmino

Istituto Italiano di Tecnologia
Genova, Italia

Giacomo Persico

Dipartimento di Energia, Politecnico di Milano
Milano, Italia
giacomo.persico@polimi.it

Darwin Caldwell

Istituto Italiano di Tecnologia
Genova, Italia

ABSTRACT

A novel concept for an air pressure-driven micro-turbine is proposed in this paper. Turbine and generator are embedded in one single component, thus eliminating coupling losses and misalignment issues, and improving compactness, reliability and lifetime. The machine is a single-stage axial impulse turbine with a rotor diameter of 14 mm. Electric and mechanical designs were carried out concurrently.

Two prototypes of the micro-turbine were built. The first one was a not fully optimized prototype for concept proofing-while the second one was designed to optimize the fluid dynamic efficiency minimizing the air consumption. In the second prototype the air flow can reach speeds up to 100000 rpm (with 2.4 bar of supply absolute pressure) and produces, when coupled to a small generator, a maximum electrical power of 13W. The maximum total efficiency is around 4% in the optimal condition while the maximum turbine efficiency is around 50%.

INTRODUCTION

The need for compact power sources and smart energy harvester is always pressing, especially for portable electronics but also for other applications. Currently electrochemical batteries are the dominant source of electrical power for compact low power applications. The main drawback of battery power is the finite supply of energy. Furthermore, in physically remote places, harvesting power from an easily available, clean and safe energy source such as compressed air may be desired. Power density increases with miniaturization and makes micro-generators truly competitive with the Lithium batteries. Miniaturization and distributed intelligence are strong drivers in this technology development.

The development of body networks, mobile and wireless computing, and vision-based telecom largely emphasized the need for performing wireless telecommunication protocols in

combination with decentralized processing units. The power requirements of such systems or even the concept of distributed power generation received relatively low attention and in most cases came down to a traditional concept of battery-operated electronics [7]. However this represents a further strategic field of application of micro-turbines. Due to the rapidly-expanding capability of micromachining technology millimeter-size range gas turbines were developed in the last decade[1].

The reduced size and mass and its higher compactness make these devices an appealing solution to power distributed sensor networks. Operational modes can range from high power/short duration (alarm, failure recovery) to low power/long duration (sensor monitoring). Possible applications are the use in distributed energy generation in remote or explosive areas without the need to wire power cable connections. Power actuation of small pneumatic valves (e.g. food process industry) can also be possible. Other uses include powering emergency and backup systems.

A number of possible solutions for micro-turbines were designed in the past with different sizes and power (a little survey is presented in Table 1): Leuven turbine (10 mm diameter, steel) [5], Tohoku turbine (4 -10 mm diameter, steel) [9], MIT turbine (4 mm diameter, silicon)[1]. The MIT group also developed a whole gas cycle starting from the idea that liquid hydrocarbon fuels have an energy density 20-30 times than the best battery technology.

Author	Institute	Year	Diameter [mm]	Speed [RPM]
S.Tanaka	Tohoku university	2003	4	1250000
S.Tanaka	Tohoku university	2009	8	642000
A.Epstein	MIT	2006	4.2	1700000
F.D.Doty	Doty Scientific	2006	4	1380000
T.Waumans	K.U.Leuven -PMA	2010	6	1200000

Table 1 Maximum speeds of some micro-turbine prototypes

These micro-turbine designs present new challenges in fluid dynamics, structural mechanics, bearing, rotor dynamics and electric machinery. A number of tradeoffs are required in order to design such systems.

This work describes the design and performance assessment of a new concept of micro-power-generator unit made by a single stage axial air pressure driven turbine and an AC three-phase generator. Traditional solutions have the turbine component coupled with the rotating part of the electric generator by means of a shaft.

The key novelty of the present design is to embed the rotor of the electrical generator and the one of the turbine in only one component. This allows eliminating coupling losses, problems due to misalignments and improving compactness, reliability and lifetime by reducing the number of components. The axial turbine is inserted in the cavity of a hollow-cylindrical-shaped permanent magnet and drives it in rotation creating a magnetic flux in the generator coils located around it, thus producing electrical energy. This solution and technology has been patented. The system is completed by an electronic equipment that controls the turbine over-speed by means of an electronic brake and performs other data communications and all the measurements.

This paper is structured as follows. After a brief survey on the advantages and technical consequences of downscaling, the main design steps are discussed. The outcome of the experimental campaign are then presented and the overall machine performance are derived, for two prototypes. The detailed analysis of the sources of losses as well as the comparison with other micro-scale technologies are finally discussed for the optimized prototype.

DOWNSCALE EFFECT

The major effect that alters the common intuitive appreciation of the behavior of micro-systems is the so-called "cube-square law" which simply reflects the fact that volumes scale with the cube of the typical length scale while areas (including surface areas) scale with the square of the length scale. When a fluidic device shrinks, surface phenomena become relatively more important than volumetric ones. The reduction of scale has several effects on the performance and construction of the turbine. Indeed the physics and mechanics influencing the design of the components do change with scale. As a consequence the optimal design can be quite different with respect to the one of standard-size turbo-machinery.

Power density

In order to keep the geometric-kinematic similarity as the machine is scaled down linearly, the air flow and thus the power decreases with the intake area (the square of the linear size) while the weight decreases with the volume of the engine (the cube of the linear size), so that the power-to-weight ratio increases linearly as the machine size is reduced [1]:

$$\left. \begin{array}{l} P \propto Q \propto A \propto L^2 \\ V \propto L^3 \end{array} \right\} \Rightarrow \frac{P}{V} \propto \frac{1}{L} \quad (1)$$

where P, Q, A, V, L are power, flow rate, area volume and linear dimension respectively. Another way to see this is that micro-size machines can be expected to operate with similar pressure ratios as their large scale counterparts, when operated at similar peripheral speeds. The micro-turbine however achieves this pressure ratio over a shorter distance than conventional turbines, which is set by the scale of the blades. The same power per unit flow rate, or inlet area, is hence achieved but over a shorter length. This reduction in length, and volume, provides the dramatic increase in power density [2].

Miniaturization also leads to extremely high rotor rotational speed (order of tens of thousands of rpm, see Table 1), lower torques, and, eventually, to high flow velocity and transonic flow regimes.

Manufacturing constraints

The small surface area to volume ratio also results in manufacturing constraints (blade profiles are limited mainly to 2D planar geometries). On the other side strength of materials increases because the machining process is more precise and, the device mass and inertia being negligibly small, the operations of fast start-up and stop become easier, making feasible the design of more sophisticated control architectures.

Viscous friction

Viscous forces in the fluid become important at small scale. Airfoil chords of the order of millimeters and room temperature inflow imply that the machine will operate at Reynolds numbers of a few tens of thousands [1]. These are small values compared to the 10^5 - 10^6 range of standard turbo-machinery. Because of the low Reynolds number, boundary layer effects play a major role in the turbine behavior and the impact of viscosity on the losses is expected to be very large.

The flow is mainly laminar and viscous friction losses come up to be 1/3 of overall losses in a high speed, high work turbo-machine (secondary flows, tip leakage, and shock wave losses account for most of the rest). The flow rate is determined by airfoil span, flow angles, and aerodynamic losses.

DESIGN OF THE SYSTEM AND COMPONENTS

Previous experiences on axial micro-turbines available in literature suggested to direct the design towards impulse axial single stage impulse turbines. The feeding air enters in the system (after regulation) by a conventional input connector. In design conditions the expansion takes place in the nozzle disk only and not across the rotor. To maximize the specific work for a given expansion ratio, the stationary blades have to deflect the flow as tangential as possible. The rotor is inserted (Fig.1) into the cavity of a hollow-cylindrical-shaped permanent magnet and drives it in rotation creating a magnetic flux in the generator coils located around it, thus producing electrical energy.

After having been discharged by the rotor blades, the air flows to the outlet naturally without any deflection through an outlet disk that has only a structural function. Indeed the rotor is supported by two high speed ball bearings (e.g. for dental

applications, DR55B ABEC 9 with ceramic rollers) one mounted on the nozzle disk and the other one mounted on the outlet disk. The diameter of the turbine is 14mm and the rotor blades, wheel and shaft are one monolithic part. Fig. 1-a and Fig. 1-b show a cut view and an exploded view of the assembly of the first micro-turbine prototype. In the cut view the main dimensions of the device are shown, while the name of the components are detailed in the exploded view:

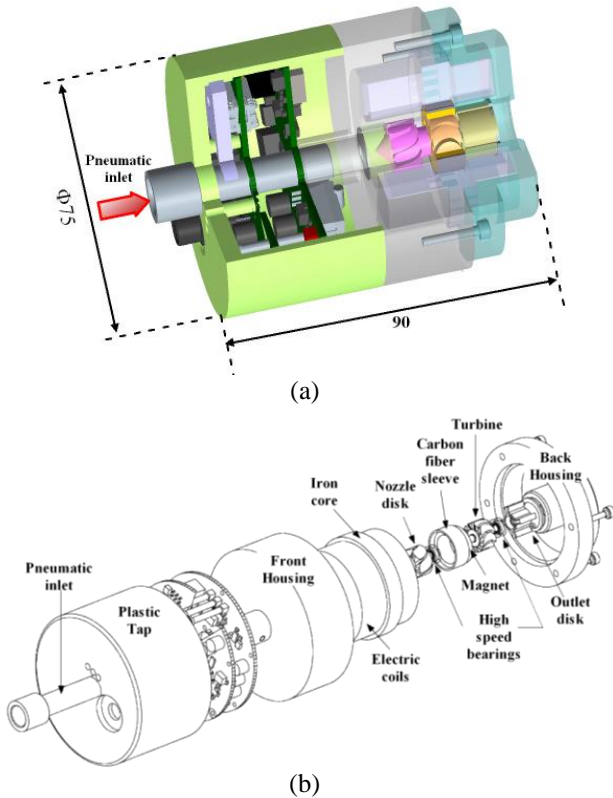


Figure 1 Micro-turbine cut view (a) and exploded view (b)

All the structural components are made in 7075 lightweight aluminum alloy (Ergal) in order to reduce the weight and to enhance heat dissipation. Particular effort was put in designing a modular mounting. A plastic tap cover contains the electronic boards that can be easily dismantled by unscrewing the inner pneumatic connector. This enables to adapt the characteristics of the system (e.g. output voltages and presence of a wireless module to send the data) to customer’s needs.

The total weight of the system is 671 g, ~40% of which is due to the housing that can be redesigned for weight reduction. The turbine main parts account only for the 3.3% of the total weight. The other heavy component is the iron core of the generator pack (38%) that, being constructed in soft magnetic steel, has the highest density. The weights of all the components are detailed in Table 2.

A number of degrees of freedom exist in the design of a system that is composed by electrical, magnetic, fluid-dynamic and mechanical components. In the present case, it was chosen to start from the electrical part and then to consider the fluid

dynamic optimization, finally studying the mechanical configuration. The design of the single components is now discussed in detail.

Components	Mass [g]	%total weight
Turbine rotor	2.3	3.3
Nozzle disk	3.2	
Outlet disk	6.1	
Magnet	9.4	
Bearings	2	
Housing (back+front)	258	38.5
Iron core+coils	256	38.3
Plastic tap	60	9
Pneumatic connector	24	3.4
Electronic boards	50	7.5
Total	670	100

Table 2 Weight of micro-turbine components

Generator

A preliminary survey on the capability to convert mechanical energy was made evaluating pros and cons. There are two main types of machines: electric machines and magnetic machines. Electric machines provide a torque that scales with the square of the rotor-stator spacing. Since rotor periphery is at very high speed, viscous drag can be very large, reducing the efficiency. Magnetic machines allow larger optimal air-gaps and thus lower drag. They are material property-limited at high temperature but this is not an issue in the present application. An off-the-shelf AC synchronous electric stator (MOOG GHD52/d10) of 52mm (external diameter) and 20mm (internal diameter) size was chosen for the present micro-turbine.

The electromagnetic torque depends on the flux coupled with the coils generated by the permanent magnet. This in turn depends on the number of coils, the length of active conductors, the number of poles, and the air-gap (if air-gap increases, the reluctance also increases and the produced magnetic flow reduces). An air gap of 0.5 mm was chosen, in order to have enough magnetic energy stored thus increasing the electromagnetic torque. In general, a high number of poles would be preferable, but eventually the number of poles was kept as low as possible to reduce the losses due to eddy currents and skin effects, and to simplify the rotational speed measurement.

A two-pole custom rotor was built for the generator. The rotor was obtained by diametrically magnetizing a hollow cylinder of neodymium permanent magnet.

Fluid-dynamic design

Scaling down dimensions including blade thickness and roughness is not feasible when going to extreme small dimensions. Indeed scaling the blade thickness proportional to the impeller diameter will lead to extreme thin blades that have an insufficient mechanical resistance to shocks or any other mechanical stress [3]. As a consequence, the blades in the present design look thicker than usual.

In a first evaluation, a reaction turbine was also considered appealing because, with respect to impulse stages, it allows to elaborate higher pressure ratios without entering in the supersonic range (because the pressure drop divides on nozzle disk and rotor). This is more compatible with industrial applications where supply pressures are normally higher than 2 bar. However for a certain pressure ratio a reaction turbine is optimized for a peripheral speed ($u=v_{II}$) that is twice the one of an impulse turbine ($u=0.5v_{II}$). The corresponding angular speed is going to be really large in comparison with the maximum range supported by the bearings; the consequent dramatic limitation of angular speed would lead to highly non-optimized designs, resulting in a very low fluid-dynamic efficiency. For this reason an axial impulse turbine was chosen.

Given the generator geometrical constraints and the volume of magnet needed to create the required flux, the external diameter of the turbine rotor was chosen to be 14mm. The length of the rotor is 8 mm to guarantee the best compromise between the friction losses and the transmitted torque.

The nozzle was designed to reach transonic flow conditions at the nozzle exit, hence with a simple converging cross-section. In absence of losses, exact sonic conditions without post-expansion are achieved for a supply pressure of 1.89 bar. The preliminary design of the stage indicated an optimum angular speed of 150000 rpm; with these data, for a vane exit angle $\alpha_1 = 10^\circ$ (measured from the tangential direction), the design rotor inlet geometrical angle would result $\beta_1 = 14^\circ$. An impulse stage being under consideration, the rotor-exit flow angle results $\beta_2 = 166^\circ$. At the initial stage of the design the blade shape resulting from these angles was considered too complex for the available manufacturing system (the prototype should be built by die-sinking EDM).

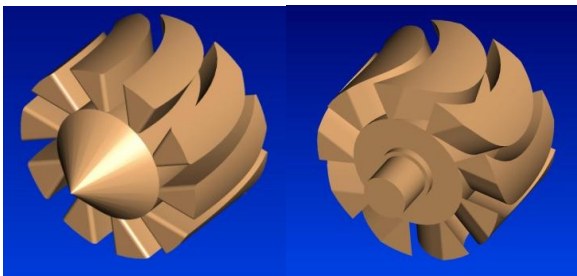


Figure 2 First prototype nozzle disk (left) and rotor (right)



Figure 3 Machined nozzle disk and rotor (1st prototype)

Due to the complexity of the task, it was preferred to carry out a step-by-step optimization, rather than to go directly through the fully coupled aerodynamic/mechanic/electric design. At first, the attention was focused on assessing the operation and performance of the electrical part, using the turbine as a prime mover. In this context, an easy-shaped machine was built (called 1st prototype in the following), characterized by a set of less severe flow angles: $\alpha_1 = 25^\circ$, $\beta_1 = 30^\circ$, $\beta_2 = 150^\circ$. Both the runner and the guide vane cascade are composed by 10 blades (or channels), whose height is equal to 2.9 mm. An axial gap of 0.5 mm was prescribed between the rotor and guide vane.

A 3D drawing of the 1st prototype is depicted in Fig. 2, as well as a picture of the assembly is provided in Fig. 3

The results of the first test were then used as a benchmark for the subsequent aerodynamic optimization that eventually led to the definition of a 2nd prototype.

Bearings

High rotating speeds require low friction bearings. Different concepts of bearings were considered:

- High speed ball bearings: commonly used in dental industry, their main advantages are the robustness and small size while their main drawbacks are the limited operating temperature and a lifetime dependent on lubrication, load and speed. To achieve higher speed other solutions without contact must be adopted.
- Static air bearings/dynamic air bearing: they levitate the rotor with air pressure either generated by an external supply (static) or by spinning the rotor (dynamic). The latter (self-acting) requires no external supply of compressed gas or energy.
- Magnetic bearings: they levitate the rotor using magnetic forces, they require sensors, actuators and control which result in high complexity and increased bearing volume.

The second and third type of bearings have no wear and therefore have a long lifetime and low losses. However magnetic bearings require sophisticated control, and are difficult to use at low scale. Static air bearings require additional air consumption, while dynamic air bearings are exposed to whirl and whip instabilities at certain speeds.

Due to the robustness, self-lubrication, small size and no need of auxiliary equipment, ball bearings were selected. High speed bearings are mostly radial, therefore axial loads can strongly affect the performances of the bearing and attention has to be paid to minimize these loads in the design. In the present machine the axial load due to the air pressure is inside the limits of the bearing. Particular attention was paid to design a mounting system that limits these loads. Ceramic spheres were used in order not to produce magnetic field leakage, and, to minimize the friction, the smallest size bearing was chosen.

Heat dissipation

Dissipation of the heat generated by the joule losses in the generator coils (that in any case are believed to be low due to the low resistivity of the coils) is provided both by the cold air

flow due to the expansion (leakage between rotor and housing can provide useful cooling of the coils) and by the aluminum materials (good thermal conductors) with which the housing bodies are built.

PERFORMANCE TESTS OF THE 1ST PROTOTYPE

The 1st prototype of the turbine has been tested for different turbine operating pressure ratios ranging from 1.5 to 2.4 by using a pressure regulator. The speed of the turbine is measured from the frequency of the generator voltage by detecting frequency zero-crossing of the back-emfs in the coils (a scheme of the test-bench is provided in Fig. 4). If the speed changes, also the operative condition and the rotor inlet relative flow angle (β_1) change, while the rotor exit flow angle (β_2) can be assumed to remain constant (determined by blades inclination), thus changing the absolute discharge flow angle (α_2). This leads to a significant change in the reaction degree and thus strongly affects the efficiency.

In the context of micro-machines detailed fluid dynamic measurements are not available and only input-output measurements can be carried out. In particular mass flow and turbine inlet temperature and pressure are recorded, that are then used (though indirectly to estimate the efficiency). Table 3 resumes the uncertainties and resolution provided by the sensors. The rectangular distribution is very commonly used when processing measurement data because specifications are often given in terms of a tolerance interval or a maximum error. In particular it is useful when dealing with readings from digital instruments [12]. Therefore uncertainty of category B for the instruments has been calculated assuming a rectangular probability distribution of the measurement errors:

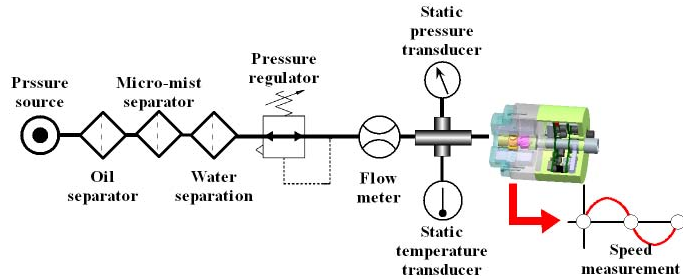


Figure 4 Test-bench schematic

The tests have been carried out at room temperature (20°C) and only slight fluctuations were observed from run to run.

Sensor	Brand/Model	Resolution/Range	Uncert. (B type)	Units
Flowmeter	SMC/PF2A751	5/0-525	±5.8	lpm
Pressure transducer	Metal work/9000600	0.01/0-10	±0.11	bar
Temp. transducer	Jumo/eTRON M	0.1/(-200)-600	±0.46	°C

Table 3: 1st prototype and 2nd prototype design parameters

Nozzle disk losses

A characterization of the aerodynamic performance of the nozzle blade row is crucial for an optimal design of the rotor, especially for impulse stages. For a fixed expansion ratio the flow velocity and the relative flow angle at the rotor inlet are indeed strongly influenced by the losses occurring upstream of the rotor. Unfortunately standard loss correlations, available for large scale turbines, are not valid for the present micro system, because of the low Reynolds number, the high roughness and the large blade thickness. The losses are expected to play a relevant role on the rotor inlet relative flow field, because of the small width of the channels and the strong weight of the boundary layers. To overcome these difficulties, and to provide more realistic data for the optimized design, experimental tests were carried out. For measuring the losses on the stationary blades only, a particular test was set-up (sketched in Fig. 5).

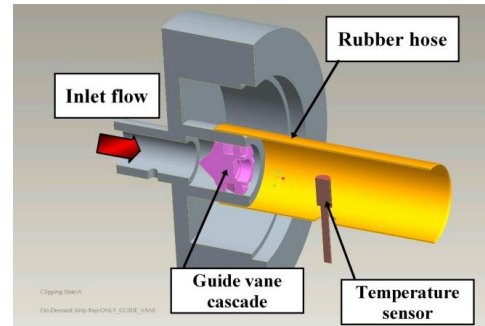


Figure 5 Test set-up for nozzle disk losses estimation

The rotor is removed and the nozzle only is considered; pressure measurements are performed in the upstream duct feeding the turbine, representing the vane inlet stagnation pressure. The stagnation temperature at the exit, equal to that at the inlet, as well as the mass flow rate are also monitored. The pressure at the nozzle exit can be assumed to be equal to the atmospheric one, as it should occur when the turbine is operated under design impulse conditions. In this way, global information on the loss and air consumption of the nozzle disk can be derived by applying the following procedure:

$$v_{1ax} = \frac{\dot{m}}{\rho_1 S_1} \quad v_{1t} = \frac{v_{1ax}}{\tan(\alpha_1)} \quad (2)$$

$$M_1 = \frac{\sqrt{v_{1ax}^2 + v_{1t}^2}}{c_1} \quad c_1 = \sqrt{\gamma RT}$$

$$p_{t1} = p_1 \left(1 + \frac{(\gamma-1)}{2} M_1^2 \right)^{\frac{\gamma}{\gamma-1}}$$

$$Y = \frac{p_{t0} - p_{t1}}{p_{t0} - p_1}$$

Some iterations were required to estimate the density at the nozzle exit, since no static temperature measurements are performed. Direct velocity measurements being not available, the gauging angle was assumed as the vane exit flow angle.

Experiments on the 1st Prototype, reported in Fig. 6, indicates good stator performance, with 7% of total pressure loss coefficient for choked flow conditions (corresponding to a total-static pressure ratio of 2). It is interesting to note that the loss coefficient progressively reduces up to sonic conditions, remaining almost constant thereafter. This behavior is explained considering that, increasing the Mach number at constant inlet temperature, also the Reynolds number increases, leading to a reduction of friction coefficient in subsonic conditions. Above choking conditions shock losses arise, balancing the positive effect of further increase in Reynolds number.

However, the flow rate at choking conditions (see Fig. 7) is more than twice of the specified target, set around 200 Nlpm.

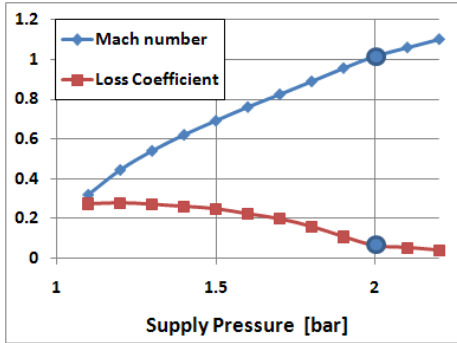


Figure 6 Nozzle blade losses and Mach number (1st prototype)

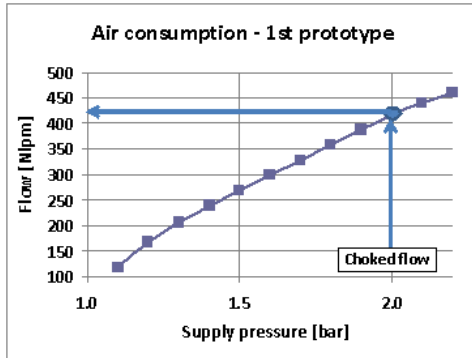


Figure 7 Nozzle disk air consumption (1st prototype)

The results of these tests state that, despite the good aerodynamic efficiency, the air consumption is too high. This means that an optimized fluid dynamic design is worthwhile.

Turbine torque and friction identification

The turbine torque was estimated according the following procedure [5]. In steady-state the torque generated by the turbine balances the friction at that speed. Therefore at a certain supply pressure it will correspond a certain turbine torque T_t and therefore a certain steady speed Ω_0 . Friction mainly occurs between the rotor and the surrounding air and in the bearings.

On the other hand, during a dynamic transient, the following equation holds:

$$T_t - T_f - T_{em} = J \frac{d\Omega}{dt} \quad (3)$$

$$T_f = k\Omega$$

Where T_t is the turbine torque, T_f the friction torque, T_{em} electromagnetic torque (zero in no load conditions) and J the moment of inertia of the rotating component (rotor+magnet). To assess the value of the torque T_t at different speeds, the friction coefficient k has to be first identified.

Hence we put in rotation the machine up to a certain steady speed and then we switched off the pressure and measure the deceleration profile. In this case the system is governed by the following differential equation:

$$-k\Omega = J \frac{d\Omega}{dt} \quad (4)$$

whose solution is the well-known exponential decay for the speed:

$$\Omega(t) = \Omega_0 e^{-\frac{k}{J}t} \quad (5)$$

where Ω_0 is the initial turbine steady speed at the instant the pressure is switched off. The test was repeated for different initial speeds (achieved with different supply pressures) from 30000 RPM to 110000 RPM in order to have a more reliable dataset for the identification (Fig. 8).

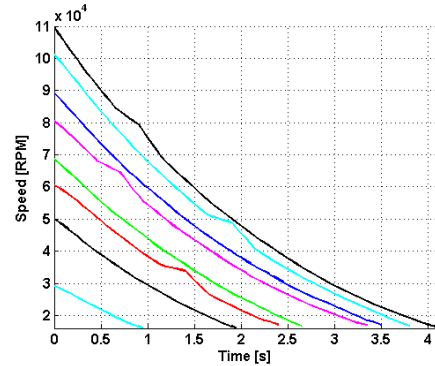


Figure 8 Deceleration tests for friction identification

The value of the moment of inertia J is 0.46 kgmm² 90% of which is due to the magnet.

The identification was carried out by Least Square Regression. Sample data has been acquired with a sample rate of 200Hz. Eq. (5) has been discretised to:

$$\Omega(t) = \underbrace{\left(1 - \frac{k\Delta T}{J}\right)}_{\theta} \Omega(t-1) \quad (6)$$

where θ is the unknown parameter, that is function of k . Next, defining φ as the matrix of regressors and building φ with the measured samples of all the data-sets and trials put in a column, yields:

$$\Omega_m(t) = \varphi\theta = \Omega_m(t-1)\theta \quad (7)$$

By computing the pseudo-inverse we identified the value of the parameter θ :

$$\theta = [\phi^T \phi]^{-1} \phi^T \Omega_m(t) \quad (8)$$

and work out value of the friction coefficient $k=2.134 \cdot 10^{-7}$ Nm/RPM.

Then the turbine was tested (again at no load condition) by supplying a different pressures and measuring the acceleration a to steady speed. The acceleration was derived by speed differentiation after a proper moving-average filtering. By summing the friction torque $k\Omega$ to the acceleration torque Ja we obtained the value of the turbine torque T_t , that is a function of the speed. We repeated the test for different supply pressures obtaining the results presented in Fig. 9:

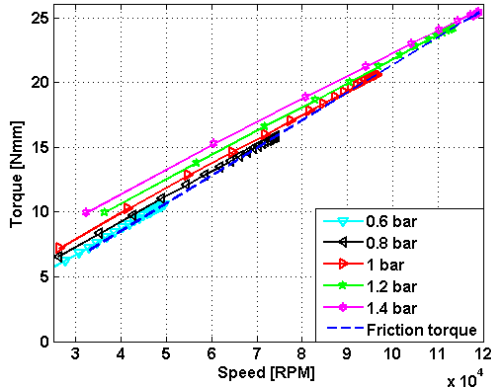


Figure 9 Torque generated by the turbine as a function of speed and supply pressure (1st prototype)

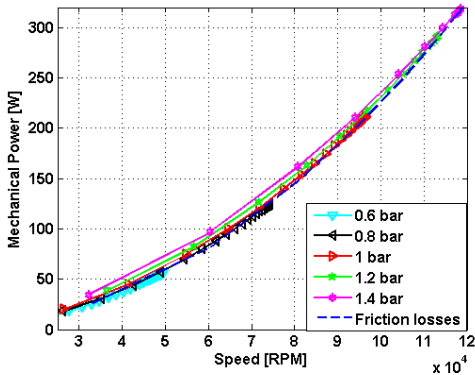


Figure 10 Mechanical power generated by the turbine as a function of speed and pressure (1st prototype)

The mechanical power was then computed by simply multiplying the torque by the speed (Fig. 10):

Turbine efficiency

The turbine total-static efficiency η_t is defined as the mechanical energy output divided by the pneumatic energy of an isentropic total-to-static expansion of the consumed air:

$$\eta_t = \frac{\Delta h_{ACT}}{\Delta h_{ISO}} = \frac{T_t \Omega}{c_p h_{t1} \left[1 - \left(\frac{p_2}{p_{t1}} \right)^{\frac{\gamma-1}{\gamma}} \right] \dot{m}} \quad (9)$$

Where c_p is the air specific heat, and h_{t1} and p_{t1} are the inlet stagnation enthalpy (derived from temperature) and pressure

respectively. The measured temperature drop could be used to derive efficiency, but this method was not considered for the relatively high uncertainty in the temperature measurements. Then the turbine efficiency in the whole range of pressure and speed is computed assuming isentropic conditions (Fig. 12):

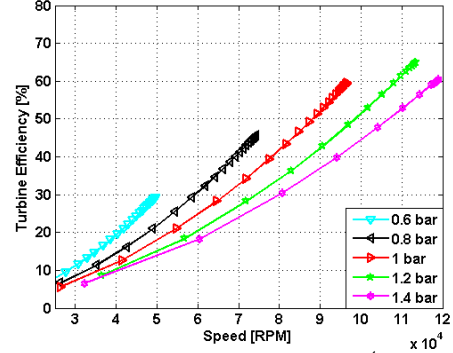


Figure 11 Efficiency of the turbine (1st prototype)

For this system, the maximum mechanical efficiency at sonic conditions ranges between 30% and 65%. The tests have been carried out without any muffler. This is because any fitting on the outlet would create pressure losses and reduce the pneumatic power available across the runner, thus affecting efficiency.

Generator efficiency

To obtain the total efficiency the generated electrical power must be assessed. The speed is controlled by varying an electric load. A variable resistive load was connected to a 3 phase diode rectifier bridge that, at the same time, is connected to the 3 coils of the generator. The resistance is changed discretely from 300Ω down to 1Ω thus changing the delivered electrical power and leading to a gradual deceleration of the turbine. Speed, voltage across the load and current are recorded and the generated electrical power computed (Fig. 12). It must be remarked that an aspect of rectification is a loss from the peak input voltage to the peak output voltage, due to the built-in voltage drop across the diodes (around 0.7 V for ordinary silicon p-n-junction diodes and 0.3 V for Schottky diodes). Bridge rectification will have a loss of two diode drops. This may represent significant power loss in very low voltage supplies. Therefore in the computation of the electrical power these losses were compensated:

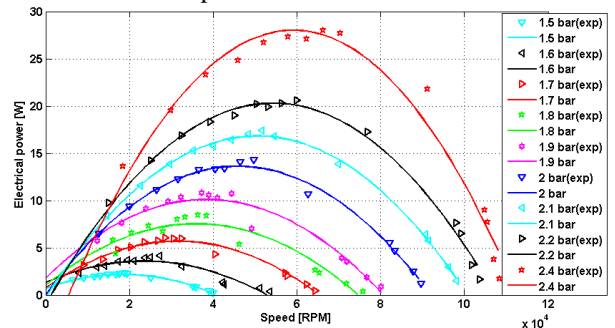


Figure 12 Electrical power generated by the system (1st prototype)

The rectified voltage V_{bulk} at no load condition varies with speed as shown in Fig 13, but acceptable values are achieved:

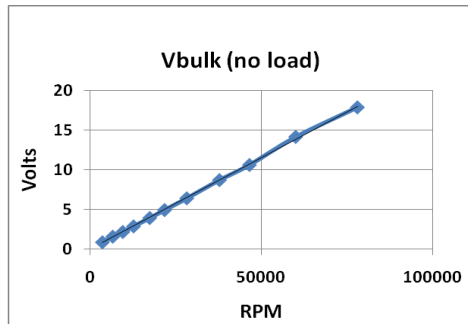


Figure 13 V_{bulk} rectified voltage

Finally by considering the consumed pneumatic power it is possible to estimate the total efficiency of the turbine (compressed air to electrical power) (Fig. 14). As is can be seen in the data, very low level of overall efficiency are achieved with the 1st prototype, hence a revised improved design is crucial for the demonstration of the technology.

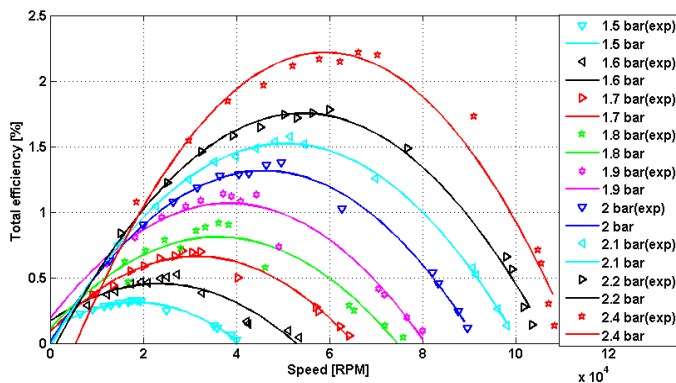


Figure 14 Total efficiency (1st prototype)

DESIGN IMPROVEMENT

2nd prototype nozzle disk

In the 1st prototype the high value of the air consumption is caused by the relatively high flow angle at the nozzle exit, that leads to a high axial velocity component ($v_{1ax}=120$ m/s). In general for any gas turbine, maximizing the net output power includes maximizing both specific power and mass flow. Specific power is sensitive to component efficiency and pressure ratio (especially at low pressure ratio such as the present one). High efficiency implies optimal airfoil design; high flow rate requires large flow areas. However industrial applications require lower air consumption than the one achieved with the 1st prototype. Nevertheless in the 1st prototype the power output is satisfactory and it would decrease if the mass flow rate is decreased. To a certain extent potential reduction of power connected to the mass flow limitation can be compensated through an increase of aerodynamic performance. Therefore the improved design followed these concurrent guidelines:

- To increase efficiency and reduce losses, by reducing incidence losses for the rotor blade row:
 - by rounding the rotor blade leading edge (thus reducing incidence losses at low angular speed);
 - by reducing machining roughness.
- To limit the air consumption, following several means:
 - by reducing the nozzle disk outlet area:
 - blade height reduction. Not feasible in the present case, the turbine external diameter being fixed by the electrical design;
 - reduction of the number of blades/channels;
 - by reducing the axial velocity component: the nozzle gauging angle α_1 is reduced from 25° to 15° (this is the most influent parameter). Theoretical studies revealed that this change would lead to a 45% reduction of the air consumption (Table 4).

In Fig. 15 the 3D drawing of a new nozzle disk is presented.

Channels	10	10	8	6
α_0 [deg]	25°	15°	15°	15°
Outlet area [mm ²]	47	59	49	35
Axial component [m/s] v_{1ax}	131	80	80	80
Flow [Nlpm]	370	282	236	168
% Flow decrease	0%	23%	36%	45%
Tangential component [m/s] v_{1t}	281	300	300	300
% Euler work increase	0%	7.1%	7.1%	7.1%

Table 4 Flow reduction and increase of work exchange for different nozzle disk designs

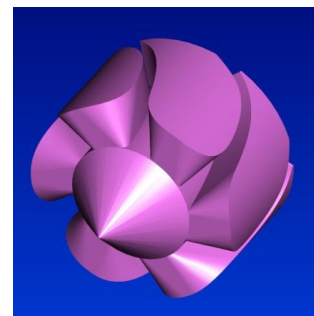


Figure 15 Nozzle disk for the 2nd prototype

Similarly to what done for the 1st prototype, preliminary tests were performed to estimate the nozzle disk performance. As expected, the severe channel geometry and the high flow deflection turns into a dramatic increase of vane losses (Fig. 16). As a result choking conditions are approached only at the maximum tested expansion ratio (2.5, corresponding to an estimated Mach number of 0.95). In this conditions a loss

coefficient of 47% is estimated. The air consumption, instead, is strongly reduced to 230 Nlpm (Fig. 17), matching the target.

The increase in nozzle losses is somehow forced by the limitation in the air consumption. However, an optimal rotor design can at least partially compensate such an effect, as discussed in the following results.

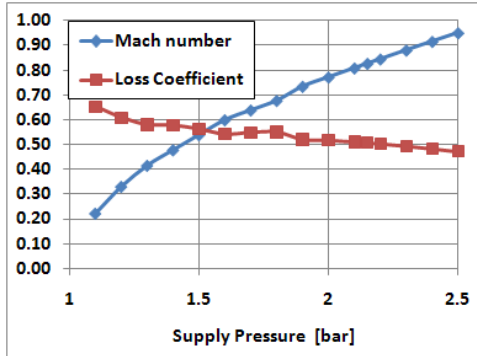


Figure 16 Nozzle disk losses and Mach number (2nd prototype)

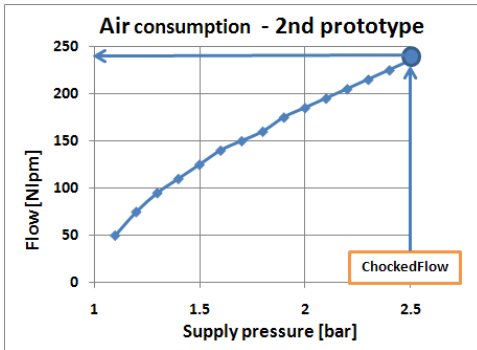


Figure 17 Nozzle disk air consumption (2nd prototype)

2nd prototype rotor

For impulse turbine stages, the exit losses (rotor discharge kinetic energy) are minimal when the turbine is designed for a u/v_{t1} ratio of 0.5, with u the peripheral speed and v_{t1} the tangential speed at the nozzle exit. On the basis of the nozzle exit measurements, the optimal angular speed for the second prototype at near choking conditions is about 250000 RPM. Unfortunately, this value is too high for the ball bearings capability. Therefore the turbine was designed to operate in impulse conditions for a $u/v_{t1} = 0.16$ ($u = 46\text{m/s}$, or $\Omega = 80000$ rpm), well below the optimal speed that would be required to minimize the discharge kinetic energy at the rotor exit. Therefore a non-negligible exit loss has to be expected.

	1 st prototype		2 nd prototype	
	Nozzle disk	rotor	Nozzle disk	rotor
α_1 [deg]	25	-	15	-
β_1 [deg]	-	30	-	14
β_2 [deg]	-	150	-	166
Number of channels	10	10	6	7

Table 5: 1st prototype and 2nd prototype design parameters

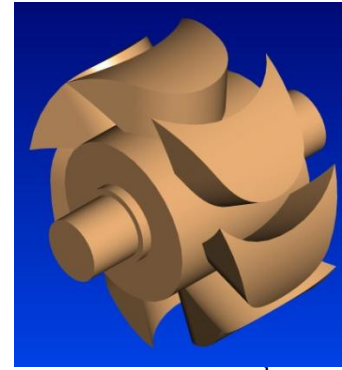


Figure 18 Turbine rotor 2nd prototype

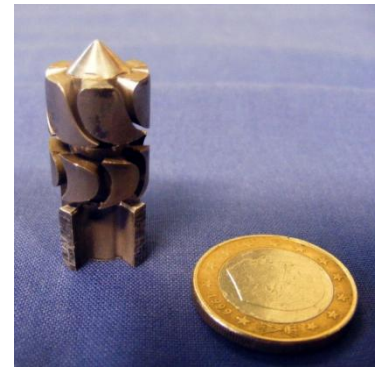


Figure 19 Machined nozzle disk and rotor (2nd prototype)

The mass flow being controlled by the nozzle, the rotor channels were designed larger than in the 1st prototype, in such a way to reduce friction and ease the machining. In Table 5 the main design parameters of the two prototypes are summarized while the 3D drawing is presented in Fig. 18. Finally in Fig. 19 a picture of the 2nd prototype is reported.

Performance tests were carried out for the 2nd prototype, with the same method and procedure used for the 1st prototype. The moment of inertia for the 2nd prototype rotor is 0.44 kgmm^2 slightly lower than the 1st one due to the larger channels. The results for the torque, the mechanical power and the turbine efficiency are depicted in Fig.20,21,22 respectively:

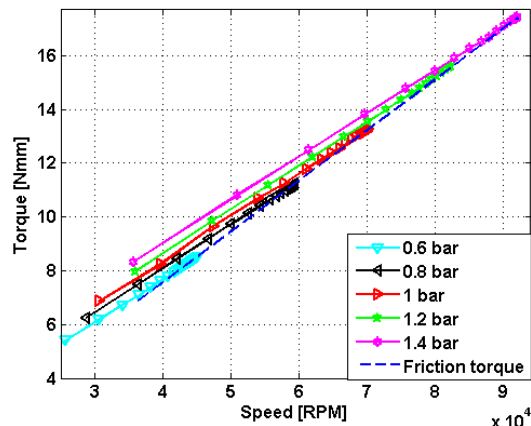


Figure 20 Torque generated by the turbine as a function of speed and supply pressure (2nd prototype)

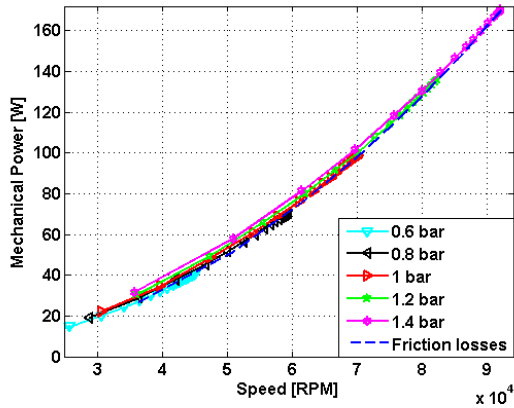


Figure 21 Mechanical power generated by the turbine as a function of speed and pressure (2nd prototype)

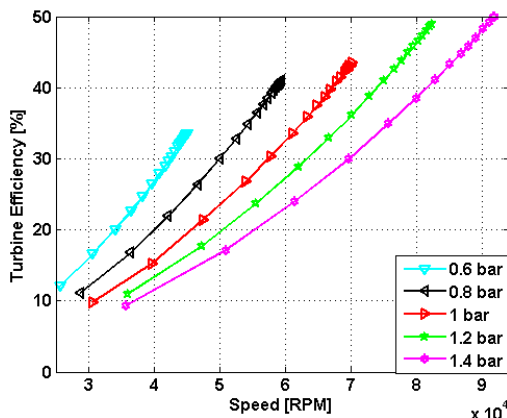


Figure 22 Efficiency of the turbine (2nd prototype) (compressed air to mechanical power)

At 80000RPM and a pressure ratio of 2.2, it can be seen that 2nd prototype mechanical power (125W) is only 17% smaller than the 1st prototype one (150W), despite the dramatic reduction in flow rate, while turbine efficiency (46%) is 35% higher than 1st prototype one (34%). These results are mainly due to the optimized blade design. The mechanical power output matches with the theoretical design calculations. Regarding the maximum electrical power produced (Fig.23), this is the half of the 1st prototype (Fig.13) while the total efficiency (Fig.24) is almost twice.

Generator performance

By considering the data of the tests at 2.4 bar, dividing the electrical power for the mechanical power the generator efficiency is obtained function of the speed (Fig.25).

As shown in Fig. 25, generator efficiency decreases as the speed increases approaching close to zero values at high speeds. Fig. 22, on the other hand, shows that turbine efficiency increases with the speed. Thus total efficiency presents a maximum located at a speed range (20000-50000RPM) lower than the rotor design speed (80000RPM). This limits the electrical output that is possible to extract by the machine. An explanation can be given by investigating the nature of the electric losses.

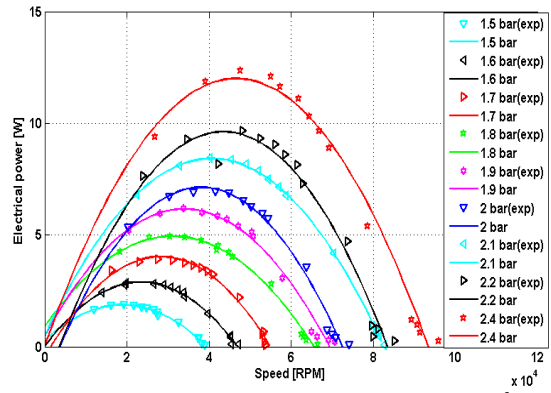


Figure 23 Electrical power generated by the system (2nd prototype)

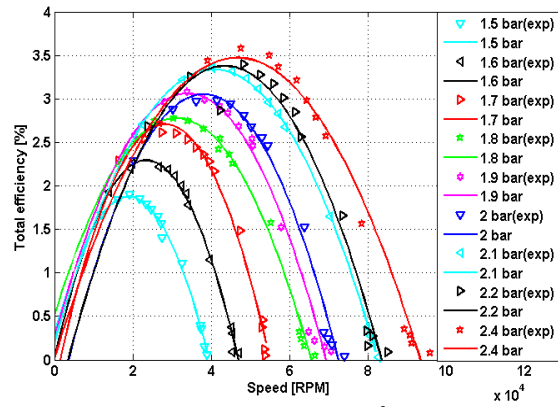


Figure 24 Total efficiency (2nd prototype)

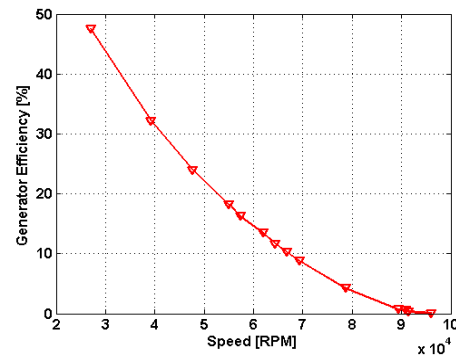


Figure 25 Generator efficiency

Generator losses turn into energy dissipation and heating of the components. Power is lost in an electrical machine through several different mechanisms:

- Resistance of the windings (copper loss),
- Magnetic friction in the core (hysteresis)
- Electric currents induced in the core (Eddy currents).

Copper losses, mainly depend on the currents and the coil resistance that in our application is very low. It is believed that the main responsible of the drop in the generator efficiency for high speeds are the core losses (hysteresis losses and Eddy currents). Indeed they are related non-linearly to the frequency. A well-known empirical approach proposed by Steinmetz a century ago is normally used for estimating hysteresis losses

[11] while Eddy currents losses, like any resistive circuit, are proportional to the square of the applied voltage that is itself proportional to the product of frequency f and induction B . Therefore the expression for these losses per unit of volume is:

$$P_{core} = P_{eddy} + P_{hyst} = K_e f^2 B_{max}^2 + K_h f B_{max}^n \quad (10)$$

Where K_i and K_h are empirical parameters obtained from experimental measurement under sinusoidal excitation (we did not characterize the core material in this work). These losses are normally reduced by adopting a thin layer stack structure for the iron block (Eddy currents) and a soft magnetic material (hysteresis) but their strong dependency on frequency make them become extremely important at high speeds. The generator electrical design is currently under investigation to improve its efficiency by reducing air gaps and re-designing coils geometry.

Sankey diagram of the losses

The Sankey diagram (Fig. 26) is a useful tool to graphically illustrate the weight that the different losses have on the system. It gives a snapshot of the energy flow and of the mechanical and electric efficiencies in a certain operating condition. We generated this diagram (for the 2nd prototype) for a supply pressure of 2.4 bar and a speed of 50000RPM, corresponding to the condition of maximum power generated and maximum efficiency (Fig.23-24). Pneumatic power, mechanical power and electric power are obtained by the previous tests. Generator losses are computed as the difference between the estimated mechanical power and the electrical output. Friction losses are obtained by the deceleration tests. Expansion losses are obtained by the nozzle alone tests, considering the reduction of kinetic energy at the vane exit between the ideal and the real expansion. Exit losses are obtained by estimating the absolute kinetic energy discharged by the rotor, from the flow rate, the relative flow angle at the rotor exit (equal to the gauging one) and the thermodynamic conditions at the rotor exit. Finally the blade losses are obtained by subtracting to the ideal pneumatic power the mechanical power, the friction losses, the expansion losses and the exit losses.

As stated previously the mechanical power produced at 50000RPM (51.5 W) is significantly lower than at the rotor design speed (130 W). Thus the electrical output is limited to 12.2 W even if the total efficiency is maximum at that speed. Conversely at 70000 RPM, close to the optimal aerodynamic condition (the blade losses are indeed dramatically reduced) the electrical output is limited by the poor electric behavior, leading to a reduction of overall efficiency and power.

A comparison of power, specific work, total efficiency and air consumption for 1st and 2nd prototype for different pressures is summarized in Table 6.

These results suggest that in future works the optimization of the electric generator is crucial to increase its efficiency at high speeds and hence to shift the maximum of the overall efficiency at higher speeds, coherently with the optimal

aerodynamic condition. In this way higher mechanical power and eventually higher electrical power should be available.

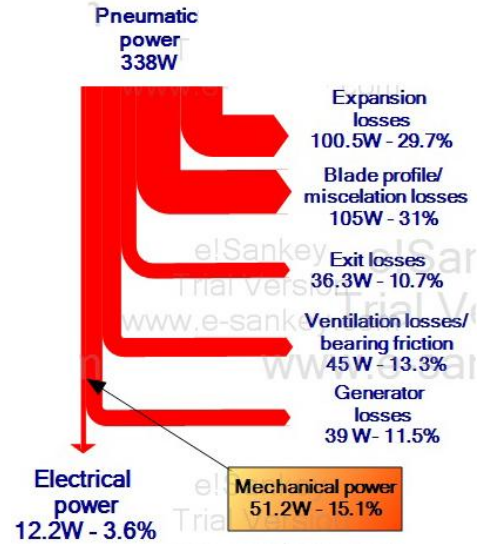


Figure 26 Sankey diagram of the losses at supply pressure of 2.4 bar, 50000 RPM

Pressure [bar]	1.6	1.8	2	2.2	2.4
Max Mech. Power 1 st prototype [W]	56	126	214	295	318
Max Mech. Power 2 nd prototype [W]	41	71	97	138	171
% decrease	-27	-43	-55	-53	-46
Flow rate 1 st prototype [Nlpm]	220	260	295	335	365
Flow rate 2 nd prototype [Nlpm]	150	175	200	220	245
% decrease	-32	-33	-32	-34	-33
Max Efficiency 1 st prototype [%]	0.3	0.8	1.31	1.7	2.2
Max Efficiency 2 nd prototype [%]	1.87	2.77	3	3.37	3.5
% increase	523	246	129	98	59

Table6: 1st prototype and 2nd prototype performance comparison

Comparison with commercial batteries

Power density is defined as the maximum power generated divided by the masses of the power generating components.

Common off the shelf lithium-ion batteries [13] can deliver a maximum current around 2250mA at a voltage of 3.6V, corresponding to a maximum power delivery of 8W, and have a power density of around 170 W/kg. At this (maximum) current this power can be delivered only for 1 hour, after that the battery must be recharged or replaced after a certain number of charges. This makes this technology a not environmentally friendly solution.

The present technology has, instead, a power density of 52 W/kg (accounting for the weight the iron pack and coils (250 g) only, since the other parts can be considered as protective enclosures and not power generating parts). There is no limit in electrical energy production as long as the air flow is provided, making the micro-turbine suitable for continuous applications. The system maintenance depends mainly on the ball bearing

failure; despite long life tests have not been carried out on them already, the bearings life is expected to be really high, since the operating speeds and loads are well below the rated limits, and the bearings are auto-lubricated.

Most of the weight is due to the iron pack (238g) therefore, by focusing on reducing the weight of this component, consistently higher values of the power density can be attained.

CONCLUSIONS AND FUTURE WORKS

A novel concept for an air-pressure driven micro-turbine has been proposed in this paper. Two prototypes were designed, built and tested. The 1st prototype, despite producing a relevant amount of electrical power, was resulting in excessive air consumption, unacceptable for industrial applications, and by very low efficiency. The design of the 2nd prototype was based on the result of the analysis carried out for the 1st one, aiming to increase efficiency and decrease air consumption. Both goals were achieved. Air consumption reduced by more than 30% while turbine efficiency increased of more than 30% in the speed range of interest (around 80000 RPM). However the usable electrical output and the total efficiency are still significantly low. The different contributions to the losses, directly measured or analytically extrapolated, have been graphically visualized in a Sankey diagram.

The main performance limitation of the proposed micro-turbine is represented by the losses in the electric generator, that becomes significantly important at high speeds.

Future works will therefore involve the characterization and the optimization of the electric generator at high speed, in order to increase the production of electrical power.

A more sophisticated, CFD-based aerodynamic optimization will also be performed, as well as the evaluation of different stage configurations suitable for low speed, like Curtis stages.

NOMENCLATURE

a	Turbine acceleration
$\alpha_1 ; \alpha_2$	Vane and rotor exit absolute angles
β_1, β_2	Rotor inlet and exit geometrical angles
c	Speed of sound
c_p	Air specific heat
γ	Ratio of specific heats
η_t	Turbine efficiency
θ	Unknown parameter in LS regression
h_{t1}	Stagnation enthalpy at vane exit
J	Moment of inertia of the rotating component
k	Friction coefficient
K_i, K_h	Empirical parameters for Eddy and hysteresis losses
\dot{m}	Mass flow
M_i	Mach number in section i
ρ	Air density
p_{ti}	Stagnation pressure in section i
p_i	Static pressure in section i
P_{core}	Total iron losses
P_{eddy}	Eddy current losses
P_{hyst}	Hysteresis losses
S_i	Discharge area in section i

T_t	Turbine torque
T_{em}	Electromagnetic torque
T_f	Friction torque
u	Peripheral speed
v_l	Vane exit absolute speed
v_{lt}	Vane exit absolute speed (tangential component)
v_{lax}	Vane exit absolute speed (axial component)
V_{bulk}	Rectified voltage
φ	Regressors matrix
Ω	Turbine angular speed
Ω_0	Turbine steady angular speed
Y	Total pressure loss coefficient

REFERENCES

- [1] Epstein, A. H., 2003. "Millimeter-scale, mems gas turbine engines", *Proceedings of ASME Turbo Expo 2003*
- [2] Fréchette, L. G., Jacobson, S. A., Breuer, K. S., Ehrich, F. F., Ghodssi, R., Khanna, R., Wong, C. W., Zhang, X., Schmidt, M. A., Epstein, A. H., 2005. "High-Speed Micro-fabricated Silicon Turbomachinery and Fluid Film Bearings", *Journal of Microelectromechanical Systems*, Vol. 14, Issue 1, pp pp. 141-152.
- [3] Van den Braembussche, R., 2005. "Micro Gas Turbines – A Short Survey of Design Problems", RTO-EN-AVT-131 Nato Research and Technology Organization, 2005.
- [4] Peirs, J., Reynaerts, D., Verplaetsen, F., 2003. "Development of an axial microturbine for a portable gas turbine generator", *Journal of Micromechanics and Microengineering*, Vol. 13, No. 5, 2003, S190-S195.
- [5] Peirs, J., Reynaerts, D., Verplaetsen, F., 2004. "A microturbine for electric power generation", *Sensors and Actuators*, Vol 113, pp 86–93
- [6] J. Peirs, P. Vleugels, T. Waumans, M. Verlinden, D. Reynaerts, F. Verplaetsen, 2004, "Development of High-Speed Bearings for Micro Gas Turbines", *15th MicroMechanics Europe Workshop (MME)*, Leuven, Belgium, 313-316.
- [7] <http://www.powermems.be/> (link active on February 2011)
- [8] Breuer, K., Ehrich, F., Fréchette, L., Jacobson, S., Lin C-C, Orr D.J., Piekos E., Savoulides N., Wong C.W., 2000. "Challenges for Lubrication in High Speed MemS", in *NanoTribology*, Edited by S. Hsu., Kluwer Press, Dordrecht
- [9] Isomura, K., 2005. "Development of Micromachine Gas Turbines at Tohoku University" RTO-EN-AVT-131, *Micro Gas Turbines, NATO Research and technology organization*.
- [10] Coey, J.M.D., 2009. "Magnetism and Magnetic Materials", *Cambridge University Press*.
- [11] Steinmetz, C.P., 1892. "On the law of hysteresis", *AIEE Transactions*, pp. 3–64, 1892. Reprinted in 1984 under the title "A Steinmetz contribution to the AC power revolution", Introduction by Brittain, J. E., *Proceedings of IEEE*, vol. 72, pp 196–221.
- [12] Taylor, J.R., 1997. "An introduction to error analysis", Oxford university press.
- [13] Panasonic Lithium-ion batteries, <http://www.panasonic.com/industrial/batteries-oem/oem/lithium-ion.aspx> (link active on February 2011)